PERGAMON

International Journal of Solids and Structures 40 (2003) 2975–2987

INTERNATIONAL JOURNAL OF SOLIDS and STRUCTURES

www.elsevier.com/locate/ijsolstr

Flexure analysis of circular elastic layers bonded between rigid plates

Hsiang-Chuan Tsai *

Department of Construction Engineering, National Taiwan University of Science and Technology, 43, Section 4, Keelung Road, P.O. Box 90-130, Taipei, Taiwan, ROC

Received 11 September 2002

Abstract

An elastic layer of circular cross-section which is bonded between rigid plates and subjected to pure bending moment is analyzed through a theoretical approach. Based on two kinematic assumptions, the governing equations for the two horizontal displacement functions are established from the equilibrium equations. The horizontal displacements are then solved by satisfying the stress boundary conditions in the elastic layer. Through these solved displacements, the vertical stress in the elastic layer, the shear stress on the bonding surfaces, and the tilting stiffness of the bonded layer are derived in closed-forms and are also compared with the results of finite element analysis.

Keywords: Bonded elastic layer; Elastomeric bearing; Flexure analysis

1. Introduction

A laminated elastomeric bearing consists of sheets of elastomer bonded to interleaving steel plates. When an elastic layer is bonded between two rigid plates, the restricted lateral expansion of the bonded surfaces of the elastic layer results in higher compression stiffness than an unbonded elastic layer. Thus, a laminated elastomeric bearing can provide high vertical rigidity to sustain gravity loading, while still providing the same horizontal flexibility of an unbonded elastomer.

To analyze the stiffness of the bonded layer, two kinematic assumptions are usually adopted: (i) planes parallel to the rigid bonding plates before deformation remain planar after loading; (ii) lines normal to the rigid bonding plates before deformation become parabolic after loading. Gent and Lindley (1959) derived the compression stiffness of an incompressible elastic layer for infinite-strip shape and circular shape. Subsequently, Gent and Meinecke (1970) extended this method to analyze the compression stiffness and tilting stiffness of incompressible elastic layers for square and other shapes.

Although rubber can be treated as incompressible in some analyses, the assumption of incompressibility tends to overestimate the compression stiffness and tilting stiffness of the bonded rubber layer when the

* Fax: +886-2-2737-6606.
E-mail address: hctsai@mail.ntust.edu.tw (H.-C. Tsai).

0020-7683/03/$ - see front matter
doi:10.1016/S0020-7683(03)00063-5

layer's shape factor (defined as the ratio of the one bonded area to the force-free area) is high. Kelly (1997) developed a "pressure solution" approach to derive the compression stiffness and the tilting stiffness considering the effect of bulk compressibility. The solutions are available for the layers of infinite-strip shape (Chalhoub and Kelly, 1991), circular shape (Chalhoub and Kelly, 1990) and square shape (Koh and Kelly, 1987).

Lindley (1979a) applied an energy method to derive the compression stiffness of the infinite-strip and circular shapes as well as the tilting stiffness of the infinite-strip shape (Lindley, 1979b) for the material of any Poisson's ratio. Koh and Kelly (1989) utilized a "variable transform" approach to derive the compression stiffness of the square shape for compressible material. Recently, Koh and Lim (2001) extended this approach to solve the compression stiffness of the rectangular shape.

The stiffness of bonded layers is related to the vertical stress, which can be derived from the mean pressure. Tsai and Lee (1998 and 1999) developed a pressure approach to derive the compression stiffness and the tilting stiffness of bonded elastic layers in infinite-strip, circular and square shapes. These solutions are accurate for the material of any Poisson's ratio. However, when using the pressure approach to derive the titling stiffness of the bonded circular layers by Tsai and Lee (1999), the horizontal displacements of the elastic layer are unable to be derived from the mean pressure, such that the shear stress distribution on the bonding surfaces of the circular layer subjected to pure bending moment cannot be studied.

In this paper, a new procedure to analyze the bonded circular layers subjected to pure bending moment is developed. Instead of directly solving the mean pressure, the governing equations of two displacement functions derived from the equilibrium equations are established, from which the horizontal displacements are solved by satisfying the stress boundary conditions of the bonded layers. The distribution of the vertical stress in the elastic layer and the shear stress on the bonding surface are then derived and compared with the finite element solutions. The derived tilting stiffness for the bonded circular layer is shown to be extremely close to the result of Tsai and Lee (1999).

2. Governing equations

A circular layer of linearly elastic, homogeneous and isotropic material bonded between two rigid plates is shown in Fig. 1. The circular layer has a diameter of $2b$ and a thickness of t. A cylindrical polar coordinate system (r, θ, z) is established with the origin at the center of the layer. Under a pure bending moment M, the rigid plates on the top and bottom of the layer rotate about the y axis (the r axis at $\theta = \pi/2$) to form

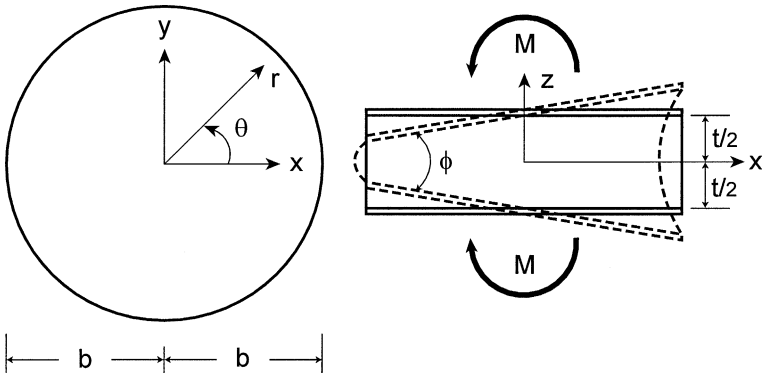

Fig. 1. Circular elastic layer bonded between rigid plates under flexure load.

an angle ϕ. Denote u, v and w as the displacements along the r, θ and z directions, respectively. The displacements are assumed to have the form

$$u(r,\theta,z) = \bar{u}(r,\theta)\left(1 - \frac{4z^2}{t^2}\right) \tag{1}$$

$$v(r,\theta,z) = \bar{v}(r,\theta)\left(1 - \frac{4z^2}{t^2}\right) \tag{2}$$

$$w(r,\theta,z) = \frac{1}{\rho} rz\cos\theta \tag{3}$$

where $\rho = t/\phi$ is the radius of bending curvature, $\bar{u}$ and $\bar{v}$ are the horizontal displacements in the middle plane of the layer. Eqs. (1) and (2) represent the kinematic assumption of quadratically varied displacements. Eq. (3) satisfies the assumption that planes parallel to the rigid plates remain planar. The expressions in Eqs. (1) and (2) are different from the displacement expressions used by Tsai and Lee (1999) which have an additional term considering the deformation of pure bending. The deformation of pure bending is quadratically varied with z, so that it can be immerged in the terms of $\bar{u}(r,\theta)$ and $\bar{v}(r,\theta)$. The expressions in Eqs. (1) and (2) ensure that the rigid plates do not have any horizontal movement.

In the cylindrical coordinate system, the mean pressure p has a relation with displacements of

$$p(r,\theta,z) = -\kappa\left(u_{,r} + \frac{u}{r} + \frac{v_{,\theta}}{r} + w_{,z}\right) \tag{4}$$

where κ is the bulk modulus, and the commas imply partial differentiation with respect to the indicated coordinates. The normal stresses and shear stresses have the following expressions

$$\sigma_{rr} = -\frac{\lambda}{\kappa}p + 2\mu u_{,r} \tag{5}$$

$$\sigma_{\theta\theta} = -\frac{\lambda}{\kappa}p + 2\mu\left(\frac{u}{r} + \frac{v_{,\theta}}{r}\right) \tag{6}$$

$$\sigma_{zz} = -\frac{\lambda}{\kappa}p + 2\mu w_{,z} \tag{7}$$

$$\tau_{r\theta} = \mu\left(\frac{u_{,\theta}}{r} + v_{,r} - \frac{v}{r}\right) \tag{8}$$

$$\tau_{rz} = \mu(u_{,z} + w_{,r}) \tag{9}$$

$$\tau_{\theta z} = \mu\left(v_{,z} - \frac{w_{,\theta}}{r}\right) \tag{10}$$

in which λ and μ are Lame's constants. For clarification, the following two displacement functions are defined

$$f(r,\theta,z) = u_{,r} + \frac{u}{r} + \frac{v_{,\theta}}{r} \tag{11}$$

$$g(r,\theta,z) = v_{,r} + \frac{v}{r} - \frac{u_{,\theta}}{r} \tag{12}$$

The equilibrium equations in the r and θ directions can be expressed as

$$2f_{,r} - \frac{g_{,\theta}}{r} + u_{,zz} + w_{,rz} = \frac{\lambda}{\kappa\mu} p_{,r} \tag{13}$$

$$g_{,r} - \frac{2f_{,\theta}}{r} + v_{,zz} + \frac{w_{,\theta z}}{r} = \frac{\lambda}{\kappa\mu} \frac{p_{,\theta}}{r} \tag{14}$$

The following average quantities through the depth are defined as

$$\bar{p}(r,\theta) = \frac{1}{t} \int_{-\frac{t}{2}}^{\frac{t}{2}} p(r,\theta,z)\,\mathrm{d}z \tag{15}$$

$$\bar{f}(r,\theta) = \frac{1}{t} \int_{-\frac{t}{2}}^{\frac{t}{2}} f(r,\theta,z)\,\mathrm{d}z \tag{16}$$

$$\bar{g}(r,\theta) = \frac{1}{t} \int_{-\frac{t}{2}}^{\frac{t}{2}} g(r,\theta,z)\,\mathrm{d}z \tag{17}$$

By using Eqs. (3) and (11), Eq. (4) becomes

$$\bar{p} = -\kappa\left(\bar{f} + \frac{r}{\rho}\cos\theta\right) \tag{18}$$

Substituting the displacement assumptions in Eqs. (1)–(3) into Eqs. (13) and (14) and integrating the resulting equations through the thickness lead to

$$\bar{u} = \frac{t^2}{8}\left[\left(\frac{\lambda+2\mu}{\mu}\right)\bar{f}_{,r} - \frac{1}{r}\bar{g}_{,\theta} + \left(\frac{\lambda+\mu}{\mu}\right)\frac{1}{\rho}\cos\theta\right] \tag{19}$$

$$\bar{v} = \frac{t^2}{8}\left[\left(\frac{\lambda+2\mu}{\mu}\right)\frac{1}{r}\bar{f}_{,\theta} + \bar{g}_{,r} - \left(\frac{\lambda+\mu}{\mu}\right)\frac{1}{\rho}\sin\theta\right] \tag{20}$$

Differentiating the multiplication of r and Eq. (19) with respect to r and then adding the result to the differentiation of Eq. (20) with respect to θ yield

$$\bar{f}_{,rr} + \frac{1}{r}\bar{f}_{,r} + \frac{1}{r^2}\bar{f}_{,\theta\theta} - \alpha^2\bar{f} = 0 \tag{21}$$

where α is defined as

$$\alpha = \sqrt{\frac{12\mu}{t^2(\lambda+2\mu)}} \tag{22}$$

Differentiating the multiplication of r and Eq. (20) with respect to r and then subtracting the result from the differentiation of Eq. (19) with respect to θ yield

$$\bar{g}_{,rr} + \frac{1}{r}\bar{g}_{,r} + \frac{1}{r^2}\bar{g}_{,\theta\theta} - \beta^2\bar{g} = 0 \tag{23}$$

where β is defined as

$$\beta = \sqrt{\frac{12}{t^2}} \tag{24}$$

3. Solution of displacements

Under the pure bending moment, the elastic layer has the following symmetric and antisymmetric properties

$$\bar{p}(r,\theta) = \bar{p}(r,-\theta) = -\bar{p}(r,\pi-\theta) \tag{25}$$

$$\bar{f}(r,\theta) = \bar{f}(r,-\theta) = -\bar{f}(r,\pi-\theta) \tag{26}$$

$$\bar{g}(r,\theta) = -\bar{g}(r,-\theta) = \bar{g}(r,\pi-\theta) \tag{27}$$

$$\bar{u}(r,\theta) = \bar{u}(r,-\theta) = -\bar{u}(r,\pi-\theta) \tag{28}$$

$$\bar{v}(r,\theta) = -\bar{v}(r,-\theta) = \bar{v}(r,\pi-\theta) \tag{29}$$

To satisfy the above conditions, the solutions of Eqs. (21) and (23) have the following expressions

$$\bar{f}(r,\theta) = \sum_{n=1,3,5,\ldots}^{\infty} A_n I_n(\alpha r)\cos n\theta \tag{30}$$

$$\bar{g}(r,\theta) = \sum_{n=1,3,5,\ldots}^{\infty} B_n I_n(\beta r)\sin n\theta \tag{31}$$

where I_n is the modified Bessel function of the first kind of order n; A_n and B_n are the constants to be determined. Substituting Eqs. (30) and (31) into Eqs. (19) and (20) gives

$$\bar{u} = \frac{t^2}{8\rho}\left(\frac{\lambda+\mu}{\mu}\right)\cos\theta + \frac{3}{2}\sum_{n=1,3,5,\ldots}^{\infty}\left\{\frac{A_n}{\alpha}\left[I_{n-1}(\alpha r) - \frac{n}{\alpha r}I_n(\alpha r)\right] - \frac{nB_n}{\beta^2 r}I_n(\beta r)\right\}\cos n\theta \tag{32}$$

$$\bar{v} = -\frac{t^2}{8\rho}\left(\frac{\lambda+\mu}{\mu}\right)\sin\theta + \frac{3}{2}\sum_{n=1,3,5,\ldots}^{\infty}\left\{-\frac{nA_n}{\alpha^2 r}I_n(\alpha r) + \frac{B_n}{\beta}\left[I_{n-1}(\beta r) - \frac{n}{\beta r}I_n(\beta r)\right]\right\}\sin n\theta \tag{33}$$

At the edge $r = b$, the normal stress in the r direction must satisfy the following condition

$$\sigma_{rr}(b,\theta,z) = 0 \tag{34}$$

By using the expression of σ_{rr} in Eq. (5) and taking integration through the depth, Eq. (34) becomes

$$\left(1+\frac{\lambda}{2\mu}\right)\bar{f}(b,\theta) - \frac{2}{3b}\left[\bar{u}(b,\theta) + \bar{v}_{,\theta}(b,\theta)\right] + \left(\frac{\lambda}{2\mu}\right)\frac{b}{\rho}\cos\theta = 0 \tag{35}$$

Substituting Eqs. (30), (32) and (33) into the above equation gives

$$\left\{\left[1+\frac{\lambda}{2\mu}+\frac{2}{(\alpha b)^2}\right]I_1(\alpha b) - \frac{1}{\alpha b}I_0(\alpha b)\right\}A_1 + \left[\frac{2}{(\beta b)^2}I_1(\beta b) - \frac{1}{\beta b}I_0(\beta b)\right]B_1 = -\left(\frac{\lambda}{2\mu}\right)\frac{b}{\rho} \tag{36}$$

for $n = 1$, and

$$\left\{\left[1+\frac{\lambda}{2\mu}+\frac{n^2+n}{(\alpha b)^2}\right]I_n(\alpha b) - \frac{1}{\alpha b}I_{n-1}(\alpha b)\right\}A_n + \left[\frac{n^2+n}{(\beta b)^2}I_n(\beta b) - \frac{n}{\beta b}I_{n-1}(\beta b)\right]B_n = 0 \tag{37}$$

for $n = 3, 5, 7, \ldots$.

The shear stress $\tau_{r\theta}$ must satisfy the following condition at the edge $r = b$

$$\tau_{r\theta}(b,\theta,z) = 0 \tag{38}$$

By using the expression of $\tau_{r\theta}$ in Eq. (8) and taking integration through the depth, Eq. (38) becomes

$$\bar{g}(b,\theta) + \frac{4}{3b}\left[\bar{u}_{,\theta}(b,\theta) - \bar{v}(b,\theta)\right] = 0 \tag{39}$$

Substituting Eqs. (31)–(33) into the above equation gives

$$\left[\frac{4}{(\alpha b)^2}I_1(\alpha b) - \frac{2}{\alpha b}I_0(\alpha b)\right]A_1 + \left\{\left[1 + \frac{4}{(\beta b)^2}\right]I_1(\beta b) - \frac{2}{\beta b}I_0(\beta b)\right\}B_1 = 0 \tag{40}$$

for $n = 1$, and

$$\left[\frac{2(n^2+n)}{(\alpha b)^2}I_n(\alpha b) - \frac{2n}{\alpha b}I_{n-1}(\alpha b)\right]A_n + \left\{\left[1 + \frac{2(n^2+n)}{(\beta b)^2}\right]I_n(\beta b) - \frac{2}{\beta b}I_{n-1}(\beta b)\right\}B_n = 0 \tag{41}$$

for $n = 3, 5, 7, \ldots$.

Eqs. (36) and (40) give the solution

$$A_1 = -\frac{\lambda b}{2\mu\rho}\alpha b\overline{A} \tag{42}$$

$$B_1 = -\frac{\lambda b}{2\mu\rho}\beta b\overline{B} \tag{43}$$

with

$$\overline{A} = \frac{\frac{4}{(\beta b)^2}\left\{\left[1 + \frac{(\beta b)^2}{4}\right]I_1(\beta b) - \frac{\beta b}{2}I_0(\beta b)\right\}}{\left\{\left[2 + \frac{(\beta b)^2}{4}\right]I_1(\beta b) - \frac{\beta b}{2}I_0(\beta b)\right\}\frac{2}{\alpha b}I_1(\alpha b) - I_1(\beta b)I_0(\alpha b)} \tag{44}$$

$$\overline{B} = \frac{\frac{2}{\beta b}\left[I_0(\alpha b) - \frac{2}{\alpha b}I_1(\alpha b)\right]}{\left\{\left[2 + \frac{(\beta b)^2}{4}\right]I_1(\beta b) - \frac{\beta b}{2}I_0(\beta b)\right\}\frac{2}{\alpha b}I_1(\alpha b) - I_1(\beta b)I_0(\alpha b)} \tag{45}$$

in which the relation between Eqs. (22) and (24) is applied. For $n = 3, 5, 7, \ldots$, Eqs. (37) and (41) give the solution

$$A_n = 0; \quad B_n = 0 \tag{46}$$

Substituting Eqs. (42), (43) and (46) into Eqs. (32) and (33) lead to

$$\bar{u} = \frac{b^2}{\rho}\left(\frac{3\lambda}{4\mu}\right)\left\{\left(1 + \frac{\mu}{\lambda}\right)\frac{2}{(\beta b)^2} - \overline{A}\left[I_0(\alpha r) - \frac{1}{\alpha r}I_1(\alpha r)\right] + \overline{B}\frac{1}{\beta r}I_1(\beta r)\right\}\cos\theta \tag{47}$$

$$\bar{v} = \frac{b^2}{\rho}\left(\frac{3\lambda}{4\mu}\right)\left\{-\left(1 + \frac{\mu}{\lambda}\right)\frac{2}{(\beta b)^2} + \overline{A}\frac{1}{\alpha r}I_1(\alpha r) - \overline{B}\left[I_0(\beta r) - \frac{1}{\beta r}I_1(\beta r)\right]\right\}\sin\theta \tag{48}$$

If the elastic layer has a Poisson's ratio $v \approx 0.5$, the magnitude of λ becomes infinite and α is infinitesimal. For a small quantity x,

$$I_0(x) \approx 1 + \frac{1}{4}x^2, \quad I_1(x) \approx \frac{1}{2}x + \frac{1}{16}x^3 \tag{49}$$

Applying these approximation, Eqs. (47) and (48) can be reduced to

$$\bar{u} = \frac{b^2}{\rho}\left(\frac{3}{16}\right)\left\{1 + \frac{8}{(\beta b)^2} - 3\frac{r^2}{b^2} + \frac{\beta b\left[\frac{I_1(\beta r)}{\beta r} - \frac{I_1(\beta b)}{\beta b}\right]}{\left[\frac{(\beta b)^2}{4} + 1\right]I_1(\beta b) - \frac{\beta b}{2}I_0(\beta b)}\right\}\cos\theta \tag{50}$$

$$\bar{v} = \frac{b^2}{\rho}\left(\frac{3}{16}\right)\left\{-1 - \frac{8}{(\beta b)^2} + \frac{r^2}{b^2} + \frac{\beta b\left[\frac{I_1(\beta r)}{\beta r} - I_0(\beta r) + \frac{I_1(\beta b)}{\beta b}\right]}{\left[\frac{(\beta b)^2}{4} + 1\right]I_1(\beta b) - \frac{\beta b}{2}I_0(\beta b)}\right\}\sin\theta \tag{51}$$

which are the horizontal displacements of the bonded circular layers of incompressible material.

The shape factor of the bonded circular layers is defined as $S = b/(2t)$, which gives, from Eqs. (22) and (24),

$$\alpha b = \sqrt{\frac{24(1-2\nu)}{1-\nu}}S, \quad \beta b = \sqrt{48}S \tag{52}$$

Therefore, it is known that the normalized horizontal displacements, $\bar{u}\rho/b^2$ and $\bar{v}\rho/b^2$ in Eqs. (47) and (48), are the functions of S, ν, r/b and θ. The normalized radial displacement at $\theta = 0$ and the normalized tangential displacement at $\theta = \pi/2$ are plotted in Figs. 2 and 3, respectively, as a function of r/b for the

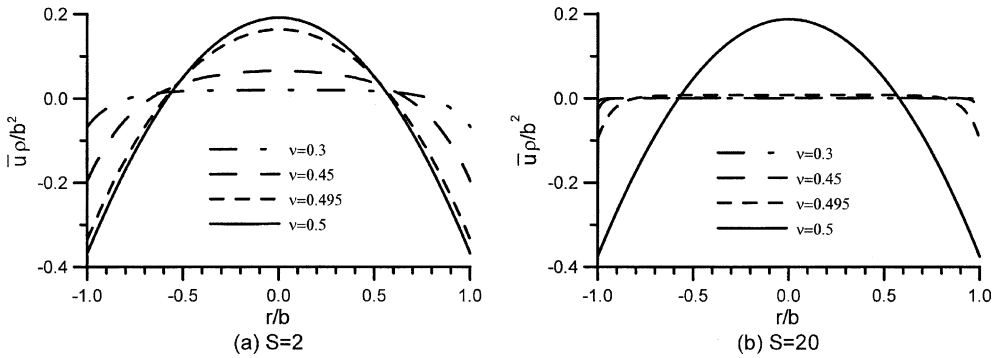

Fig. 2. Radial displacement varied with radial distance at $\theta = 0$.

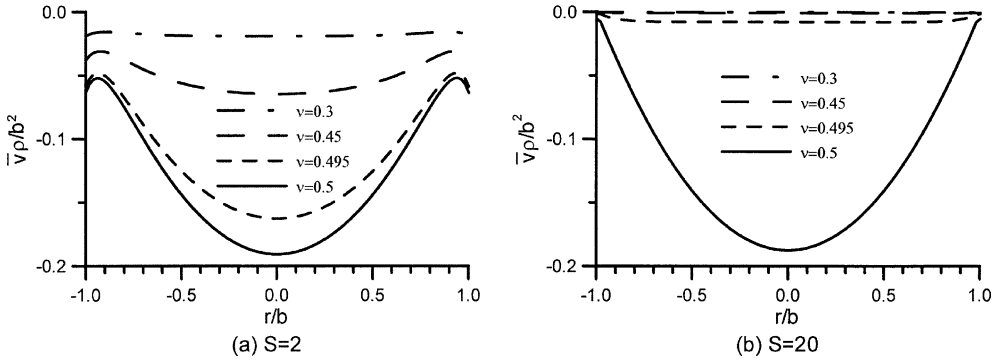

Fig. 3. Tangential displacement with radial distance at $\theta = \pi/2$.

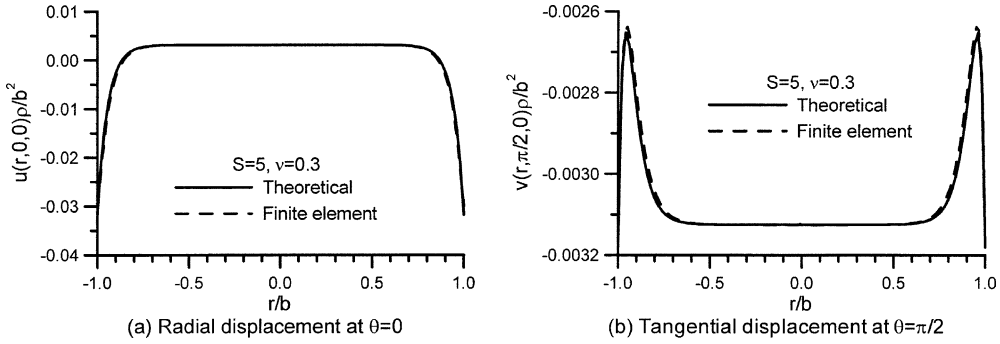

Fig. 4. Horizontal displacements in middle plane varied with radial distance.

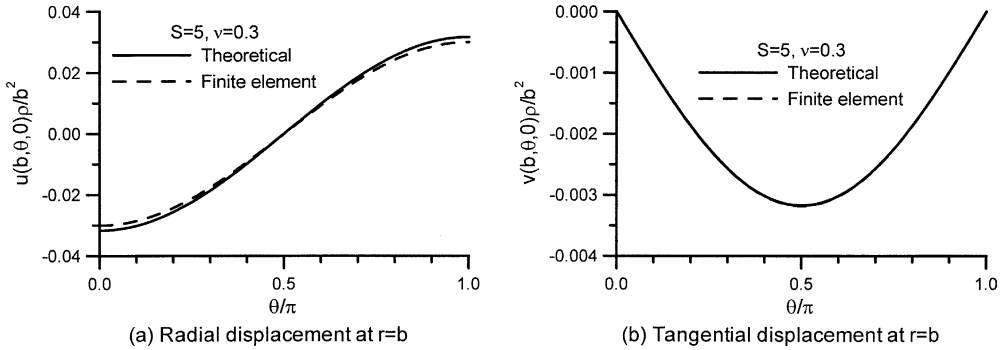

Fig. 5. Horizontal displacements in middle plane varied with angle.

shape factors of 2 and 20 with several Poisson's ratios. For the bonded layer of lower Poisson's ratio, the horizontal displacements become smaller and are more uniformly distributed along the radial direction. For the bonded layer of high shape factor ($S = 20$), the displacements differ greatly between incompressible material ($v = 0.5$) and nearly incompressible material ($v = 0.495$).

The deformation of the bonded circular layer is also analyzed by the finite element method. In the finite element analysis, the circular layer is modeled by 8-node solid elements with incompatible bending modes. The horizontal displacements calculated by the finite element method at the middle plane ($z = 0$) of the layer with $S = 5$ and $v = 0.3$ are compared with the theoretical solutions of Eqs. (47) and (48) in Figs. 4 and 5 as functions of r and θ, respectively, which show that the finite element solutions are very close to the theoretical solutions.

4. Tilting stiffness

The effective bending modulus for the bonded elastic layer is defined as

$$E_b = \frac{\rho M}{I_r} \tag{53}$$

where $I_r = \pi b^4/4$ is the moment of inertia of the plane area about the r axis. The bending moment M has the form

$$M = \int_0^b \int_0^{2\pi} \bar{\sigma}_{zz} r^2 \cos\theta \, \mathrm{d}\theta \, \mathrm{d}r \tag{54}$$

where $\bar{\sigma}_{zz}$ is the effective vertical stress defined as

$$\bar{\sigma}_{zz} = \frac{1}{t} \int_{-\frac{t}{2}}^{\frac{t}{2}} \sigma_{zz} \, \mathrm{d}z \tag{55}$$

By using the solutions of A_n in Eqs. (42) and (46), $\bar{p}$ has the form, from Eqs. (18) and (30),

$$\bar{p} = -\kappa \frac{b}{\rho} \left[\frac{r}{b} - \frac{\lambda}{2\mu} \alpha b \overline{A} I_1(\alpha r) \right] \cos\theta \tag{56}$$

Substituting Eq. (7) into Eq. (55) and using Eqs. (3) and (56) lead to

$$\bar{\sigma}_{zz} = \lambda \frac{b}{\rho} \left[\left(1 + \frac{2\mu}{\lambda} \right) \frac{r}{b} - \frac{\lambda}{2\mu} \alpha b \overline{A} I_1(\alpha r) \right] \cos\theta \tag{57}$$

From this, the effective bending modulus has the solution

$$E_b = 2\mu + \lambda - \left(\frac{\lambda^2}{\mu} \right) \frac{\frac{8}{(\beta b)^2} \left[1 + \frac{(\beta b)^2}{4} - \frac{\beta b I_0(\beta b)}{2 I_1(\beta b)} \right] \left[\frac{\alpha b I_0(\alpha b)}{2 I_1(\alpha b)} - 1 \right]}{2 + \frac{(\beta b)^2}{4} - \frac{\beta b I_0(\beta b)}{2 I_1(\beta b)} - \frac{\alpha b I_0(\alpha b)}{2 I_1(\alpha b)}} \tag{58}$$

When αb tends to infinitesimal, the following function of αb in Eq. (58) may be approximated by

$$\frac{\alpha b I_0(\alpha b)}{2 I_1(\alpha b)} \approx 1 + \frac{1}{8} (\alpha b)^2 - \frac{1}{192} (\alpha b)^4 \tag{59}$$

Consequently, the effective bending modulus of the bonded circular layer for incompressible material is

$$E_b = \frac{E}{3} \left[4 + \frac{(\beta b)^2}{24} - \frac{\frac{(\beta b)^2}{8}}{1 + \frac{(\beta b)^2}{4} - \frac{\beta b I_0(\beta b)}{2 I_1(\beta b)}} \right] \tag{60}$$

in which E is the elastic modulus of the layer. The value of the last term in the bracket is between 0.5 ($\beta b = \infty$) and 1 ($\beta b = 0$). Eq. (60) can be approximated by

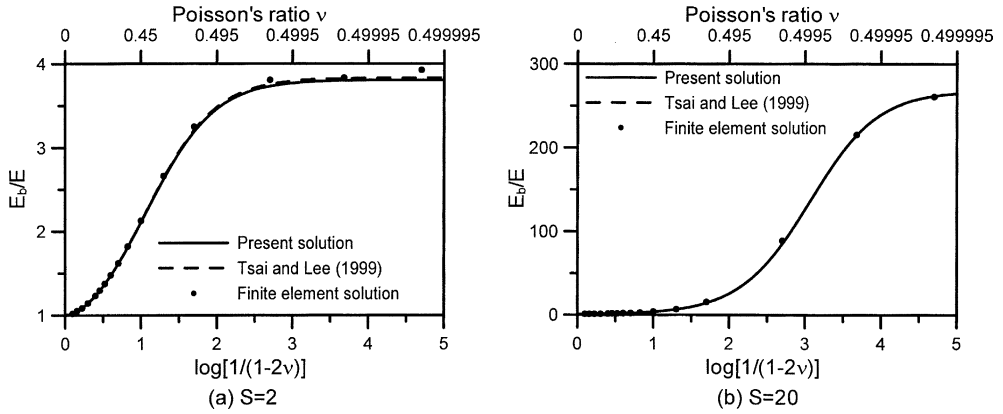

Fig. 6. Effective bending modulus of bonded circular layers varied with Poisson's ratio.

$$E_b = \frac{E}{3}\left(3.5 - \frac{1}{7S} + 2S^2\right) \tag{61}$$

which is applicable for $S \geqslant 1$.

According to Eq. (52), it is known that the normalized bending modulus E_b/E is a function of Poisson's ratio and shape factor. The curves of the bending modulus calculated from Eq. (58) varied with v for $S = 2$ and 20 are plotted in Fig. 6, which show that, when compared with the finite element solution and the solution of Tsai and Lee (1999), the bending moduli calculated by the three methods are nearly the same. When using the pressure approach, Tsai and Lee (1999) made an assumption that the tangential displacement on the edge of the middle plane of the layer is zero at the rotation axis. By means of the present approach, this assumption becomes unnecessary.

5. Stress distribution

The effective vertical stresses calculated from Eq. (57) are plotted in Fig. 7 as a function of r/b at $\theta = 0$ for the shape factors of 2 and 20 with several Poisson's ratios. In this figure, the vertical stress is normalized by bE_b/ρ which is the maximum bending stress according to the elementary beam theory. The curves of $v = 0.5$ are calculated from

$$\bar{\sigma}_{zz} = \frac{bE}{3\rho}\left\{4 + \frac{(\beta b)^2}{8}\left[1 - \frac{r^2}{b^2} - \frac{1}{1 + \frac{(\beta b)^2}{4} - \frac{\beta b I_0(\beta b)}{2I_1(\beta b)}}\right]\right\}\frac{r}{b}\cos\theta \tag{62}$$

which can be derived from Eq. (57). Unlike the distribution derived by the elementary beam theory, the vertical stress in the bonded layer is not a linear function of the radial distance. The figure indicates that the location of the maximum vertical stress is closer to the edge for the material of lower Poisson's ratio.

The in-plane shear stresses can be derived by substituting the displacement assumptions in Eqs. (1)–(3) into Eqs. (9) and (10) and using the solutions of $\bar{u}$ and $\bar{v}$ in Eqs. (47) and (48). On the bonding surface between the elastic layer and the rigid plate ($z = t/2$), the shear stresses in the radial and tangential directions have the forms as

$$\tau_{rz}(r,\theta,t/2) = 6\lambda S\frac{b}{\rho}\left\{-\frac{2}{(\beta b)^2} + \overline{A}\left[I_0(\alpha r) - \frac{I_1(\alpha r)}{\alpha r}\right] - \overline{B}\frac{I_1(\beta r)}{\beta r}\right\}\cos\theta \tag{63}$$

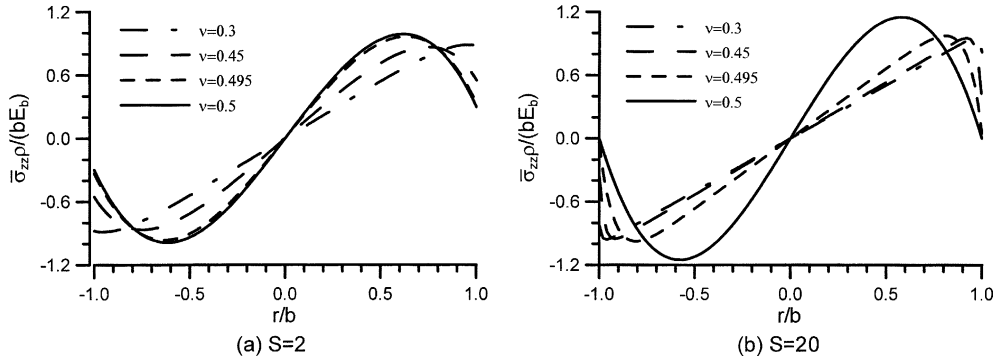

Fig. 7. Effective vertical stress with radial distance at $\theta = 0$.

$$\tau_{\theta z}(r,\theta,t/2)=6\lambda S\frac{b}{\rho}\left\{\frac{2}{(\beta b)^2}-\overline{A}\frac{I_1(\alpha r)}{\alpha r}+\overline{B}\left[I_0(\beta r)-\frac{I_1(\beta r)}{\beta r}\right]\right\}\sin\theta \tag{64}$$

When α is infinitesimal, applying the approximation in Eqs. (49) to (63) and (64) leads to

$$\tau_{rz}(r,\theta,t/2)=\frac{ESb}{2\rho}\left\{-1+3\frac{r^2}{b^2}-\frac{\beta b\left[\frac{I_1(\beta r)}{\beta r}-\frac{I_1(\beta b)}{\beta b}\right]}{\left[\frac{(\beta b)^2}{4}+1\right]I_1(\beta b)-\frac{\beta b}{2}I_0(\beta b)}\right\}\cos\theta \tag{65}$$

$$\tau_{\theta z}(r,\theta,t/2)=\frac{ESb}{2\rho}\left\{1-\frac{r^2}{b^2}-\frac{\beta b\left[\frac{I_1(\beta r)}{\beta r}-I_0(\beta r)+\frac{I_1(\beta b)}{\beta b}\right]}{\left[\frac{(\beta b)^2}{4}+1\right]I_1(\beta b)-\frac{\beta b}{2}I_0(\beta b)}\right\}\sin\theta \tag{66}$$

which are the bonding shear stresses for the elastic layer of incompressible material.

The bonding shear stress in the radial direction at $\theta=0$ and the bonding shear stress in the tangential direction at $\theta=\pi/2$ are plotted in Figs. 8 and 9, respectively, as functions of r/b for the shape factors of 2 and 20 with several Poisson's ratios, which indicate that, for the bonded layer of lower Poisson's ratio, the bonding shear stresses have a more uniform distribution over the central part.

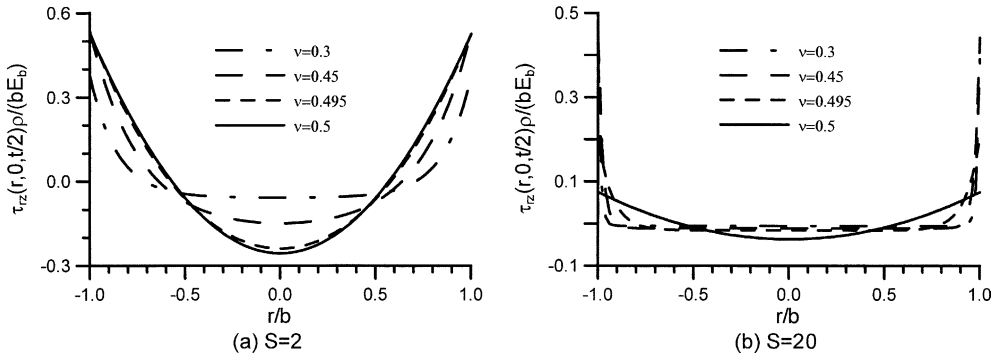

Fig. 8. Bonding shear stress in radial direction varied with radial distance at $\theta=0$.

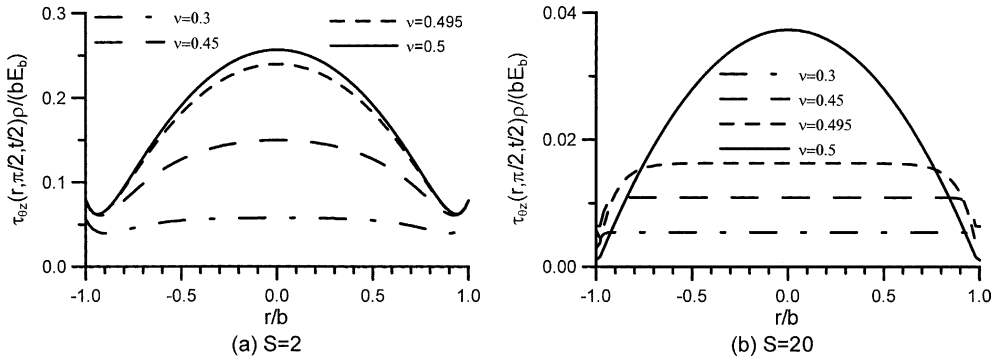

Fig. 9. Bonding shear stress in tangential direction varied with radial distance at $\theta=\pi/2$.

The comparison of the bonding shear stresses between the finite element solutions and the theoretical solutions calculated from Eqs. (63) and (64) is depicted in Fig. 10 for $S = 5$ and $v = 0.3$. For the bonding shear stress in the radial direction, the theoretical solution is very close to the finite element solution except the edge. For the bonding shear stress in the tangential direction, both solutions have the similar distribution. Because the stress in the tangential direction is much smaller than the stress in the radial direction, numerical error of the finite element analysis induces the bonding shear stress in the tangential direction to have a larger deviation between two solutions.

The maximum shear stress resultant on the bonding surface, $\tau_{\max}$, is equal to $\tau_{rz}(b, 0, t/2)$, that is,

$$\tau_{\max} = \frac{b}{\rho}\lambda S \frac{\frac{24}{(\beta b)^2}\left[1 + \frac{(\beta b)^2}{4} - \frac{\beta b I_0(\beta b)}{2I_1(\beta b)}\right]\left[\frac{\alpha b I_0(\alpha b)}{2I_1(\alpha b)} - 1\right]}{2 + \frac{(\beta b)^2}{4} - \frac{\beta b I_0(\beta b)}{2I_1(\beta b)} - \frac{\alpha b I_0(\alpha b)}{2I_1(\alpha b)}} \tag{67}$$

For the layer of incompressible material, from Eq. (65),

$$\tau_{\max} = \frac{b}{\rho} ES \tag{68}$$

The magnitude of $\tau_{\max}\rho/(bE)$ is a function of Poisson's ratio and shape factor, which is depicted in Fig. 11. $\tau_{\max}$ increases with increasing Poisson's ratio but reaches the plateau at a lower Poisson's ratio for the layer

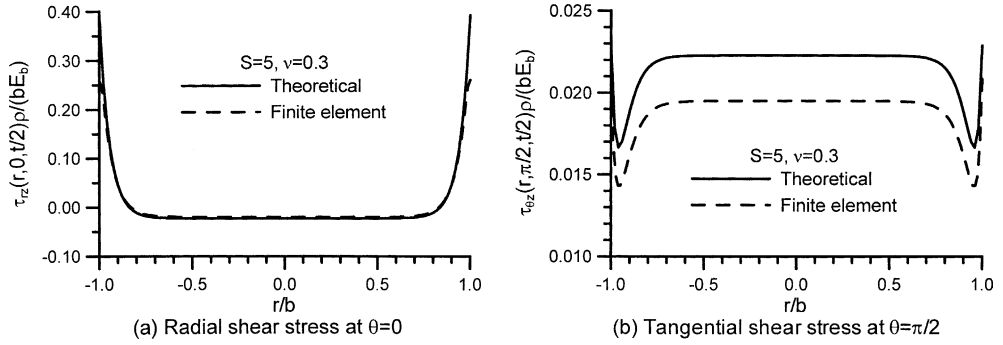

Fig. 10. Bonding shear stresses between theoretical solution and finite element solution.

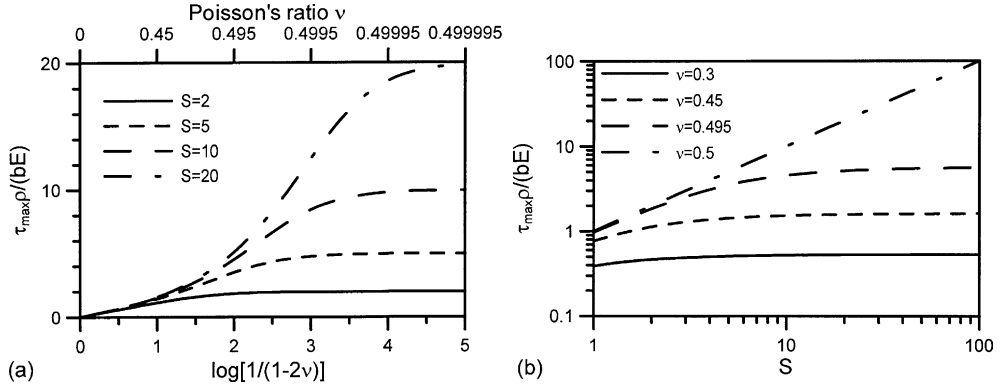

Fig. 11. Maximum shear stress resultant on bonding surfaces.

of smaller shape factor, so that τ_{max} is more sensitive to the variation of shape factor for a material of higher Poisson's ratio. When the material is incompressible, τ_{max} varies linearly with the shape factor.

6. Conclusion

Based on the two kinematic assumptions, i.e. horizontal planes remain planar and vertical lines become parabolic after deformation, the circular elastic layers bonded between two rigid plates and sustaining a pure bending moment are analyzed through a theoretical approach to find the closed-form solutions of horizontal displacements in the bonded layers. The displacements in the radial and tangential directions are shown to be proportional to $\cos\theta$ and $\sin\theta$, respectively, and not contain any higher term of Fourier series. The tilting stiffness of the bonded circular layer derived from these displacements is very close to the previous research result where an additional constraint assumption is necessary to obtain the stiffness. The analysis has no limitation on Poisson's ratio so that the effect of Poisson's ratio on the behavior of the bonded layer can be studied. When the material of the bonded layer has a lower Poisson's ratio, the shear stress on the bonding surface has a smaller magnitude and a more uniform distribution over the central part.

Acknowledgement

The research work reported in this paper was supported by the National Science Council, Republic of China, under grant no. NSC89-2211-E011-059. This support is greatly appreciated.

References

Chalhoub, M.S., Kelly, J.M., 1990. Effect of bulk compressibility on the stiffness of cylindrical base isolation bearings. International Journal of Solids and Structures 26, 734–760.

Chalhoub, M.S., Kelly, J.M., 1991. Analysis of infinite-strip-shaped base isolator with elastomer bulk compression. Journal of Engineering Mechanics, ASCE 117, 1791–1805.

Gent, A.N., Lindley, P.B., 1959. The compression of bonded rubber blocks. Proceeding of the Institution of Mechanical Engineers 173, 111–117.

Gent, A.N., Meinecke, E.A., 1970. Compression, bending and shear of bonded rubber blocks. Polymer Engineering and Science 10, 48–53.

Kelly, J.M., 1997. Earthquake-Resistant Design with Rubber, second ed. Springer-Verlag, London.

Koh, C.G., Kelly, J.M., 1987. Effects of axial load on elastomeric isolation bearings. Report no. UCB/EERC-86/12. Earthquake Engineering Research Center, University of California, Berkeley.

Koh, C.G., Kelly, J.M., 1989. Compression stiffness of bonded square layers of nearly incompressible material. Engineering Structures 11, 9–15.

Koh, C.G., Lim, H.L., 2001. Analytical solution for compression stiffness of bonded rectangular layers. International Journal of Solids and Structures 38, 445–455.

Lindley, P.B., 1979a. Compression module for blocks of soft elastic material bonded to rigid end plates. Journal of Strain Analysis 14, 11–16.

Lindley, P.B., 1979b. Plane strain rotation module for of soft elastic blocks. Journal of Strain Analysis 14, 17–21.

Tsai, H.-C., Lee, C.-C., 1998. Compressive stiffness of elastic layers bonded between rigid plates. International Journal of Solids and Structures 35, 3053–3069.

Tsai, H.-C., Lee, C.-C., 1999. Tilting stiffness of elastic layers bonded between rigid plates. International Journal of Solids and Structures 36, 2485–2505.